[14]"Waterjet Propulsion System Study. Report Number 3: Internal Flow Tests," Rept. LR 17885-3, 1965, Lockheed California Co., Burbank, Calif.

[15]"Waterjet Propulsion System Study. Report Number 5: System Design and Analysis," Rept. LR 17885-5, 1965, Lockheed California Co., Burbank, Calif.

[16]Wallis, G. B., *One-Dimensional Two-Phase Flow*, McGraw-Hill, New York, 1969, pp. 244–246.

[17]Hinze, J. O., "Fundamentals of the Hydrodynamic Mechanism of Splitting in Dispersion Processes," *A.I.Ch.E. Journal*, Vol. 1, No. 3, Sept. 1955, pp. 289–295.

[18]Tangren, R. F., Dodge, C. H., and Seifert, H. S., "Compressibility Effects in Two-Phase Flow," *Journal of Applied Physics*, Vol. 20, No. 7, July 1949, pp. 637–645.

[19]Mottard, E. J. and Shoemaker, C. J., "Preliminary Investigation of an Underwater Ramjet Powered by Compressed Air," TN D-991, Dec. 1961, NASA.

[20]Muir, J. F. and Eichhorn, R., "Compressible Flow of an Air-Water Mixture Through a Vertical, Two-Dimensional, Converging-Diverging Nozzle," *Proceedings of the 1963 Heat Transfer and Fluid Mechanics Institute*, Stanford University Press, Stanford, Calif. 1963, pp. 183–204.

[21]Witte, J. H., "Predicted Performance of Large Water Ramjets," unpublished work, Hydronautics, Inc., Laurel, Md., 1969.

[22]Vliet, G. C. and Leppert, G., "Forced Convection Heat Transfer from an Isothermal Sphere to Water," *Journal of Heat Transfer*, Vol. 83, May 1961, pp. 163–175.

[23]Sclichting, H., *Boundary Layer Theory*, McGraw-Hill, New York, 1968, p. 108.

[24]Bird, R. B., Stewart, W. E., and Lightfoot, E. N., *Transport Phenomena*, Wiley, New York, 1960, p. 192.

[25]Haberman, W. L. and Morton, R. K., "An Experimental Investigation in the Drag and Shape of Air Bubbles Rising in Various Liquids," D.T.M.B. Rept. 802, Sept. 1953, Dept. of the Navy, Washington, D.C.

[26]Gouse, S. W., Jr. and Brown, G. A., "A Survey of the Velocity of Sound in Two-Phase Mixtures," 64-WA/FE-35, Nov. 1965. American Society of Mechanical Engineers, New York.

[27]Henry, R. E., Grolmes, M. A., and Fauske, H. K., "Propagation Velocity of Pressure Waves in Gas-Liquid Mixtures," *Cocurrent Gas-Liquid Flow*, Plenum Press, New York, 1969, pp. 1–18.

[28]Kreyszig, E., *Advanced Engineering Mathematics*, Wiley, New York, 1962, pp. 92–94.

APRIL 1973 J. HYDRONAUTICS VOL. 7, NO. 2

Dynamic Response of Marine Propellers to Nonuniform Flowfields

Hideya Tsushima*
and
Maurice Sevik†
The Pennsylvania State University, University Park, Pa.

The necessity to reduce propeller-induced ship vibrations has led to the adoption of skewed blades. Such blades are more flexible than conventional ones and respond dynamically to the nonuniform velocity field generated by a ship's hull. The resulting time-dependent hydrodynamic and inertial loads may either alleviate or magnify the over-all forces and couples exerted by the propeller. These hydroelastic effects have been analyzed theoretically and verified experimentally on a model propeller.

Nomenclature

$A(\phi_\alpha,\bar{m})$ = integrand of lift operator
f = time-dependent load acting on a blade element
F = time-dependent hydrodynamic load due to nonuniform inflow velocity field
J = number of radial strips subdiving each blade
$K(\ )$ = kernel function of integral equation
$L(\ )$ = spanwise hydrodynamic load function
M_k = generalized mass corresponding to the kth mode of vibration
Δp = unsteady hydrodynamic pressure acting on the blade surface
P = hydrodynamic force due to dynamic response of the blades
q = order of blade harmonic
r_0 = tip radius of propeller
r_h = hub radius of propeller
s = width of radial strip
S = area of blade surfaces
t = time
U = volume mean velocity = $\dfrac{\int_0^{2\pi}\int_{r_h}^{r_0} V(r,\phi)r\,dr\,d\phi}{\pi(r_0^2 - r_h^2)}$
$V(r)$ = Fourier component of wake velocity normal to the blade
$w(X,r,\phi;t)$ = self-induced velocity at a control point at time t
X,r,ϕ = cylindrical coordinate system of control point
α_k,β_k = mode shape factors associated with the kth natural frequency
$\beta(r)$ = pitch angle of blade at radial position r
γ_q = phase angle of blade harmonic
$\delta(\rho,\theta;t)$ = deformation function of the blade at time t
$\Delta_k(\omega)$ = amplitude of the normal coordinates cooresponding to the kth mode of vibration
η = loss of factor of blade material
$\theta_b{}^r$ = projected propeller semichord length at radius r
ι = $(-1)^{1/2}$
ξ,ρ,θ = cylindrical coordinate system of loading point
Ξ_k = generalized force corresponding to the kth mode of vibration
$\xi_k(t)$ = normal coordinate associated with the kth mode of vibration
ρ_f,ρ_R = mass density of fluid and propeller blade material, respectively
σ^r = angular measure of skew at radius r
$\psi_k(\rho,\theta)$ = normalized mode shape of the blade corresponding to the kth natural frequency
ω = angular frequency
$(\cdot)$ = differentiation with respect to time

Subscripts
$(\ )$ = vector quantity, printed in boldface type
$(\ )_0$ = initial position of control point in propeller plane
$(\ )_\alpha$ = angular chordwise location of control point

Received August 7, 1972.
Index category: Propulsion System Hydrodynamics.

*Graduate Assistant, Department of Aerospace Engineering.

†Professor of Aerospace Engineering, and Director, The Garfield Thomas Water Tunnel; Ordnance Research Laboratory; presently Associate Technical Director, Naval Ship Research and Development Center, Carderock, Md. Associate Fellow AIAA.

Introduction

AN important problem in ship design concerns the vibrations generated by the propeller. Due to its response to a spatially and temporally nonuniform velocity field within

which it operates, the propeller exerts time-dependent axial and side forces, as well as fluctuating torques and moments upon the hull of a ship.

In recent years, the aforementioned forces and couples have been the subject of much theoretical and experimental research. In particular, unsteady lifting surfaces theories such as that of Tsakonas[2] have been developed and accurately predict experimental results, in many cases.

The necessity for minimizing unsteady forces and, hence, ship vibration levels, however, has led to the adoption of propeller blades with a high degree of skew. Such blades are more flexible than conventional ones so that hydroelastic effects cannot be ignored. The dynamic response of the blades may either alleviate or worsen the net forces and couples. This is the motivation behind the present study.

The problem has been approached by extending the linearized three-dimensional lifting surface theory of Tsakonas to include the elastic deformation of the blades. The predictions have been verified experimentally on a three-bladed, skewed propeller used by Boswell[5] in a previous investigation. Good agreement between predicted and measured values of the forces have been observed.

Equations of Forced Motion of an Elastic Blade

A propeller operating in a spatially nonuniform inflow velocity field experiences a distributed load $\mathbf{f}$ which includes three components

$$\boldsymbol{f}(\rho,\theta;t) = \boldsymbol{F}(\rho,\theta;t) + \boldsymbol{P}(\rho,\theta;t) - \rho_R(\rho,\theta)\,\ddot{\boldsymbol{\delta}}(\rho,\theta;t) \quad (1)$$

The time-dependent force $\mathbf{F}$ represents the load which an ideally rigid propeller of identical geometry would experience if it were subjected to the same flowfield. The dynamic response of the blades of a real propeller gives rise to an additional hydrodynamic force $\mathbf{P}$ as well as to an inertial force $\rho_R\ddot{\delta}$. In order to find the over-all vibratory forces, torques and moments which act upon the propeller at any instant of time, it is necessary to integrate $\mathbf{f}$ over-all blade elements.

The magnitude of the unknown deformation function δ can be expressed as a summation of the products of the normal modes of vibration of the blades ψ and normal coordinates ξ as follows

$$\delta(\rho,\theta;t) = \sum_{k=1}^{\infty} \psi_k(\rho,\theta)\,\xi_k(t) \quad (2)$$

The application of well-known methods leads to a set of coupled, linear differential equations of motion for the normal coordinates ξ_k of the form

$$M_k\ddot{\xi}_k + \omega_k^2(1+\iota\eta)M_k\xi_k = \Xi_k^D + \Xi_k^M, \quad k = 1,2,3\ldots \quad (3)$$

where

$$M_k = \int_S \rho_R \Psi_k^2\, dS = \text{generalized mass}$$

ω_k = natural frequency corresponding to the kth mode of vibration and η = loss factor of the blade material;

$$\Xi_k^D = \int_S \Psi_k R\, dS = \text{generalized force due to the disturbing nonuniform flowfield}$$

$$\Xi_k^M = \int_S \Psi_k P\, dS = \text{generalized force resulting from the dynamic response of the propeller blades}$$

The generalized forces are hydrodynamic in nature and can be calculated independently of each other. In particular, the generalized force corresponding to a rigid propeller can be predicted by means of an existing theory, such as that of Brown[1] or that of Tsakonas, Jacobs and Rank.[2] The approach adopted in the present work follows that of Ref. 2.

The unknown hydrodynamic loading which acts on a blade surface element can be expressed in terms of an integral equation which relates the self-induced velocity w to the pressure distribution on the lifting surfaces, namely

$$w(X,r,\phi_0;t) = -\int_S \Delta p(\xi,\rho,\theta_0)\,K(X,r,\phi_0;\,\xi,\rho,\theta_0;l)\,dS \quad (4)$$

where K = kernel function representing the velocity induced at a control point on the blade located at (X,r,ϕ_0) by an oscillatory pressure of unit amplitude at a loading point on the blade located at (ξ,ρ,θ_0); Δp = unknown hydrodynamic pressure acting on the blade surface.

The boundary conditions require that the self-induced velocity be equal and opposite to the velocity distribution normal to the propeller blades. For a rigid propeller, we require

$$w(X,r,\phi_0;t) = -V(r)e^{\iota q(\Omega t - \phi_0)} \quad (5)$$

where $V(r)$ = Fourier component of the wake velocity normal to the blade at a radial distance r from the hub centerline; Ω = angular velocity of the propeller; q = order of blade harmonic.

If the blades are flexible, however, the self-induced velocity must also counteract a component due to blade vibrations. The linearized boundary condition in this case is given by

$$w(X,r,\phi_0;t) = [(\partial/\partial t) + U\cot\beta(r)(\partial/r\partial\phi_0)]\,\delta(X,r,\phi_0;t) \quad (6)$$

where $\beta(r)$ = pitch angle of the blade at a radial position r; U = mean volume velocity. The numerical integration of Eq. (4) is difficult to perform because of the strong singularities of the kernel function K. Schemes for simplifying and evaluating the kernel were devised by Watkins, Woolston and Cunningham[3] in connection with oscillating wings in subsonic flow. They replaced the unknown load distribution by a sum of functions which possess the general character of the expected hydrodynamic loadings. The chordwise pressure distribution was represented by a Birnbaum series which satisfies the Kutta condition at the trailing edge and has the proper leading edge singularity. As a result of this substitution, Eq. (4) reduces to a sum of definite integrals with unknown coefficients whose magnitudes determine the spanwise lift distribution. These integrals are evaluated numerically by satisfying the downwash distribution given by Eqs. (5) and (6) at a discrete number of control points located on the blades. This approach was successfully used by Tsakonas, Jacobs and Rank[2] in their unsteady lifting surface theory for marine propellers. Their analysis leads to a set of simultaneous algebraic equations relating the unknown spanwise hydrodynamic load function L to the self-induced velocity w. A necessary simplification consisted in subdividing each blade into J radial strips and assuming the spanwise distribution of loading to be constant on each element. In addition, the number of chordwise hydrodynamic modes is restricted to $\bar{n}$ and, hence, there are $\bar{n}$ simultaneous equations of the form

$$\frac{1}{\pi}\int_0^{\pi} A(\phi_\alpha,\bar{m})\,\frac{w(r_i,\phi_\alpha;t)}{U}\,d\phi_\alpha = -\frac{e^{\iota\omega t}}{4\pi\rho_f U^2}\sum_n\sum_j L^{(\bar{n})}(\rho_j)K^{(\bar{m},\bar{n})}(r_i,\rho_j) \quad (7)$$

where $\phi_{i\alpha}$ = angular chordwise position of a control point; r_i = radial position of a control point; ρ_j = radial position

of a loading point; $\bar{m} = 1, 2, \ldots \bar{n}$, $i = 1, 2, \ldots \bar{J}$, $j = 1, 2, \ldots \bar{J}$.

The integrands of the lift operators which appear on the left-hand side of Eq. (7) have the form

$$A(\phi_{\alpha},1) = 1 - \cos\phi_{\alpha},\ \bar{m} = 1,\ A(\phi_{\alpha},2) = 1 + 2\cos\phi_{\alpha},$$
$$\bar{m} = 2, A(\phi_{\alpha},\bar{m}) = (\cos(\bar{m}-1)\phi_{\alpha}(\bar{m}-1),\ \bar{m} = 2$$

The kernel $K^{(\bar{m},\bar{n})}$ has been derived in Ref. 2. Expressions for this quantity are given in Appendix A.

Since the inflow velocity field is temporally steady, all events at a point located on the propeller will vary with a frequency $\omega = q\Omega$. Consequently, the normal coordinates have a time-dependence given by

$$\xi_k(t) = \Delta_k(\omega)e^{\iota\omega t} \tag{8}$$

The major steps in calculating the values of the admittances $\Delta_k(\omega)$ are as follows: first, the boundary conditions given by Eqs. (5) and (6) are substituted in Eq. (7) and the hydrodynamic loading functions are expressed in terms of $\Delta_k(\omega)$. The generalized forces are next found and substituted in Eq. (3). The resulting set of simultaneous algebraic equations are then solved for $\Delta_k(\omega)$. This process, which is described in detail in Ref. 4, is outlined below.

First the generalized force due to the dynamic response of the blades will be established. In order to simplify the calculations, the chordwise profile of the blades is assumed to remain undistorted by the vibratory motion. As a result, the mode shapes corresponding to the kth natural frequency can be expressed as follows

$$\Psi_k(r,\phi_{\alpha}) = \alpha_k(r)\cos\phi_{\alpha} + \beta_k(r) \qquad k = 1,2,3\ldots \tag{9}$$

$\alpha_k(r)$ and $\beta_k(r)$ are functions of the radius only. The angle ϕ_{α}, which represents the angular position of a control point, has the value of zero at the leading edge ot a blade and of π at its trailing edge.

We now substitute Eq. (9) into Eq. (2) and find an expression for the boundary condition on the blades from Eq. (6). In performing this step, the angle ϕ_0 which occurs in Eq. (6) and which denotes the initial position of a control point in the propeller plane is replaced by $[\sigma^r - \theta_b{}^r \cos\phi_{\alpha}]$, where σ^r is an angular measure of skewness at radius r and $\theta_b{}^r$ represents the projected semichord length of the propeller at radius r.

From Eq. (7) we can now obtain the values of the hydrodynamic loading functions in terms of Δ_k. This equation is given in matrix form as follows

$$\{L^{(\bar{n})}(\rho)\}^M = -4\pi\rho_f U^2 [K]^{-1}[J]\{\Delta\} \tag{10}$$

In this equation, $\{L^{(\bar{n})}(\rho)\}^M$ is a column matrix composed of $\bar{m}$ rows. The superscript M indicates that the unknown hydrodynamic spanwise modes are associated with the motions of the blades resulting from their elastic deformations. $[K]^{-1}$ is an $\bar{m} * \bar{m}$ square matrix of the kernel whose elements are given in Appendix A. The matrix $[J]$ is rectangular and has $\bar{m}$ rows and k columns, where k denotes the vibration mode number. Finally, $\{\Delta\}$ is a column matrix having k rows. The elements of the $[J]$ matrix are given by

$$J^{(1,k)}\theta_b{}^r{}_i) = \frac{\alpha_k \cot\beta(r_i)}{r_o r_i\ \theta_b{}^r{}_i} + \iota\frac{qa}{r_o}\left[-\frac{\alpha_k}{2} + \beta_k\right]$$

$$J^{(2,k)}\theta_b{}^r{}_i) = \frac{\alpha_k \cot\beta(r_i)}{r_o r_i\ \theta_b{}^r{}_i} + \iota\frac{qa}{r_o}(\alpha_k + \beta_k) \tag{11}$$

$$J^{(3,k)}\theta_b{}^r{}_i) = 0,\quad J^{(\bar{m},k)}(q\,\theta_b{}^r{}_i) = 0$$

where $a = r_0\Omega/U$ and r_0 = propeller tip radius.

After some simple steps, the following expression for the generalized force is obtained

$$\Xi_k^M = -8\pi s\rho_f U^2\,[\alpha\beta]_k[K]^{-1}[J]\{\Delta\} \tag{12}$$

where s = width of radial strips into which the blades are subdivided. The row matrix $[\alpha\beta]_k$ has $\bar{m}$ columns whose elements are given by

$$[\alpha\beta]_k = [\beta_k(\rho) +$$
$$1/2\,\alpha_k(\rho);\ 1/2\,\beta_k(\rho);\ 1/8\,\beta_k(\rho);\ 0;\ 0;\ \ldots;\ 0] \tag{13}$$

The generalized force $\Xi_k{}^D$ due to the nonuniform flowfield can be found in an analogous manner. It is given by

$$\Xi_k^D = 8\pi s\rho_f U^2[\alpha\beta]_k\,[K]^{-1}\,[I]\left\{e^{-\iota(q\sigma^r+\gamma_q)}\ \frac{V_q(r)}{U}\ \cos\beta(r)\right\} \tag{14}$$

where γ_q = phase angle of the wake harmonic q.

The elements of the row matrix $[I]$ are given in Appendix A.

With the generalized forces thus determined, the equations of motion (3) can be written in dimensionless form as follows

$$\frac{q^2}{8\pi}\left(\frac{r_0}{s}\right)\left(\frac{\Omega r_0}{U}\right)^2\left(\frac{M_k}{\rho_f r_0{}^3}\right)\left\{(1+\iota\eta)\left(\frac{\omega_k}{q\Omega}\right)^2 - 1\right\}\left(\frac{\Delta_k}{r_0}\right) =$$
$$-\frac{1}{r_0{}^2}\,[\alpha\beta]_k\,[K]^{-1}\,[J]\{\Delta\} +$$
$$\frac{1}{r_0{}^2}\,[\alpha\beta]_k\,[K]^{-1}\quad\left\{\frac{V_q(r)}{U}\cos\beta(r)\,e^{-\iota(q\sigma^r+\gamma_q)}\right\} \tag{15}$$

Equation (15) constitutes a set of simultaneous equations which can be solved for the admittance $\Delta_k(\omega)$.

At this stage useful engineering information can be obtained. It can readily be shown[4] that the combined load distribution along the span of the blades reduces to

$$\{L(\rho)\}^{D+M} = \{L^{(1)}(\rho)\}^D + 1/2\,\{L^{(2)}(\rho)\}^D$$
$$+ \{L^{(1)}(\rho)\}^M + 1/2\,\{L^{(2)}(\rho)\}^M \tag{16}$$

The thrust and torque fluctuations are given in terms of this combined loading function by the real part of Eqs. (17) and (18), respectively,

$$T_F(q) = -Ne^{\iota q\Omega t}\int_{\rho}\{L(\rho)\}^{D+M}\cos\beta(\rho)\,d\rho \tag{17}$$

$$Q_F(q) = -Nr_0e^{\iota q\Omega t}\int_{\rho}\{L(\rho)\}^{D+M}\,\rho\,\sin\beta(\rho)\,d\rho \tag{18}$$

where N = number of blades on the propeller; $\beta(\rho)$ = geometric pitch angle of the blades at radius ρ. Similar, somewhat more complicated expressions for the side forces and moments, are given in Ref. 4.

Equation (15) shows that the following dimensionless parameters must be kept constant if geometrically similar propellers are to generate the same thrust, torque and moment coefficients 1) $\omega_k/q\Omega$ = ratios of the kth natural frequency of the blade to the frequency of excitation; 2) η = material loss factor; 3) $(M_k/\rho_f r_0{}^3)$ = ratio of the generalized mass associated with the kth mode of vibration of the blade to a mass of liquid; 4) $\Omega r_0/U$ = a flow coefficient proportional to the propeller's advance coefficient; 5) $V_q(r)/U$ = ratio of the Fourier coefficient of the wake velocity to the volume mean velocity.

If these parameters are kept constant, then the value of Δ_k/r_0 in Eq. (15) will be the same, irrespective of propeller size and material properties. The right-hand side of

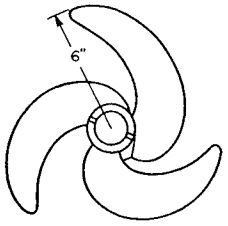

Fig. 1 Geometric configuration of skewed propeller (NSRDC No. 4143).

Eq. (10) for the spanwise loading

$$\frac{1}{\frac{1}{2}\pi\rho_f U^2 r_0^2}\{L^{(\bar{n})}(\rho)\}^M = -\frac{8}{r_0^2}[K]^{-1}[J]\{\Delta\}$$

will, therefore, also be the same. Consequently, the unsteady thrust, torque and moment coefficients will all be identical.

As an example, imagine that the unsteady thrust coefficient of a full-scale propeller is to be determined experimentally by means of a model which is L times smaller. To satisfy similarity requirements, the model must be made of the same material as the full-scale propeller so as to maintain the same value of the loss factor η and mass ratio $M_k/(\rho_f r_0^3)$. It must be tested in the same fluid medium. Since the natural frequency ω_k of the model will be L times larger than that of the full-scale propeller, the rpm must also be increased by this factor. Thus, the ratio $\omega_k/(q\Omega)$ will be constant. A constant flow coefficients $(\Omega r_0/U)$ implies that identical values of the various coefficients (such as the thrust and torque coefficient) will be obtained at a velocity U which will be the same for both model and full-scale propellers. In addition, the inflow velocity field, which is characterized by $V_q(r)/U$ must be geometrically similar.

Some additional parameters which do not appear in Eq. (15) must also be mentioned. The first is the Reynolds number which should be high enough to prevent laminar separation. Secondly, cavitation must be avoided. Thirdly, the tests must be performed at or close to the zero thrust advance coefficient of the propeller, since the theory does not account for the effects of steady loading.

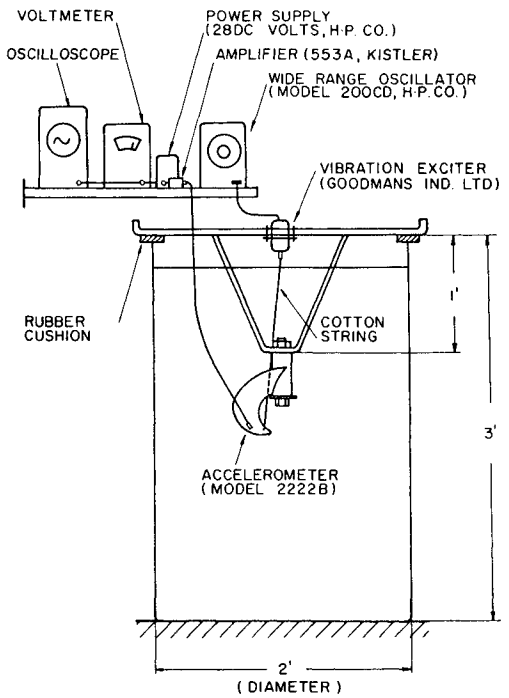

Fig. 2 Measurement of the natural frequencies of the epoxy resin blade in water.

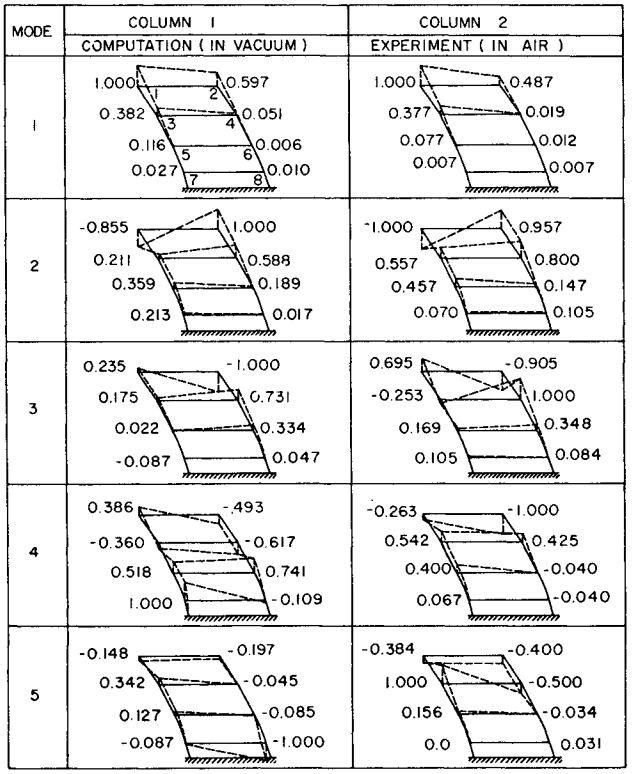

Fig. 3 Normal vibration mode shapes of the skewed propeller blade.

As a specific example, consider the thrust fluctuation ratios shown in Fig. (8). These apply to a model propeller, 1 ft in diam, described later in this paper. The frequency at which the peak response is obtained on a geometrically similar propeller which is 10 ft in diameter and is made of brass is equal to 10.5 Hz. For a three-bladed propeller, this corresponds to 210 rpm.

Application of the Theory to a Three-Bladed Skewed Propeller

In order to verify the theory experimentally, a specific model propeller shown in Fig. 1 was selected. This had been tested by Boswell[5] in a previous investigation. It was designed at the Naval Ship Research and Development Center, and is designated by NSRDC 4143. It has an expanded area ratio of 0.6 and 120° of skew. The thrust coefficient is equal to 0.150 at a design advance ratio of 0.833. It has a tip radius r_0 of 6 in. and is made of aluminum alloy.

For experimental purposes a second, identical propeller was made in epoxy resin. This material has a mass density of 0.078 lb/in.^{3}, a modulus of elasticity of 1.43×10^6 lb/in.^{2} and a loss factor of 2.5×10^{-2} at room temperature. With this choice of materials, a wide difference in the amplitudes of the unsteady thrust and torque of the

Table 1 Natural frequencies of vibration of epoxy resin blades

Mode no.	Frequency, Hz Air	Water
1	118	46.3
2	321	130
3	496	258
4	676	333
5	712	426

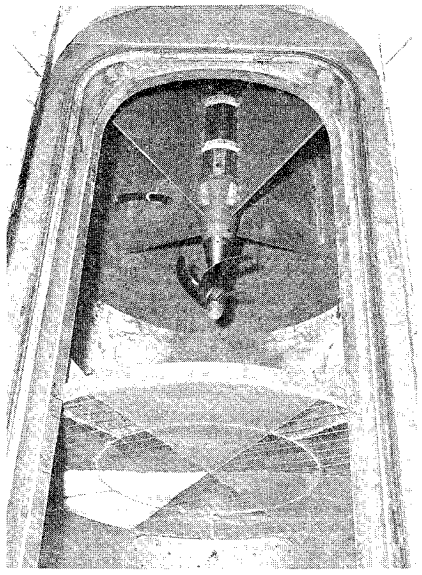

Fig. 4 Propeller and balance mounted in the water tunnel test section behind a three-cycle wake screen.

metal and plastic propellers were predicted within the planned operating range of the tests. First the natural frequencies and mode shapes of the epoxy resin blades were measured, in air and then in water. The test set-up is shown in Fig. 2. Three Endevco model 2222B microminiature accelerometers weighing 0.5 g each were used to map the blade deflections. The results are given in Fig. 3 and Table 1.

Next, the spanwise loading distribution was calculated numerically. For this purpose, each blade was divided into $\bar{J} = 8$ equal radial strips. The propeller advance ratio was equal to 1.15, which corresponds to a small steady thrust force. The inflow velocity field corresponded to one generated by a three-cycle wake screen, as shown in Fig. 4. The characteristics of the flowfield at a distance of 30 in. downstream of the screen is shown in Fig. 5. This position coincided with the propeller plane during the tests.

One result of these calculations is shown in Fig. 6. The real and imaginary parts of the unsteady thrust force of an ideally rigid propeller—in this case, the aluminum alloy

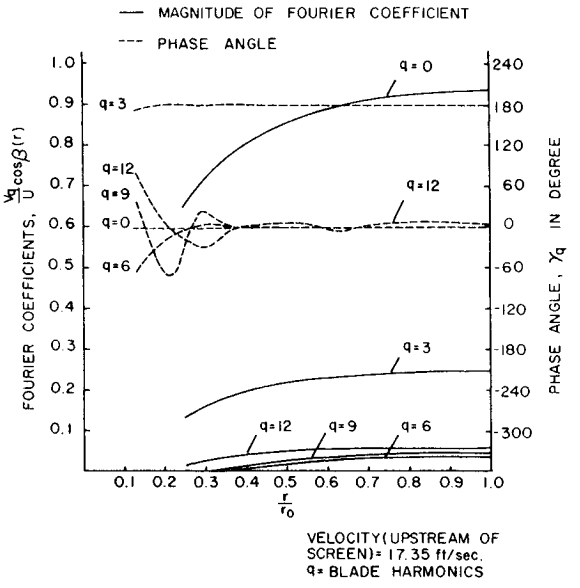

Fig. 5 Fourier coefficients of the flow downstream of the three-cycle wake screen normal to the pitch datum line for propeller No. 4143.

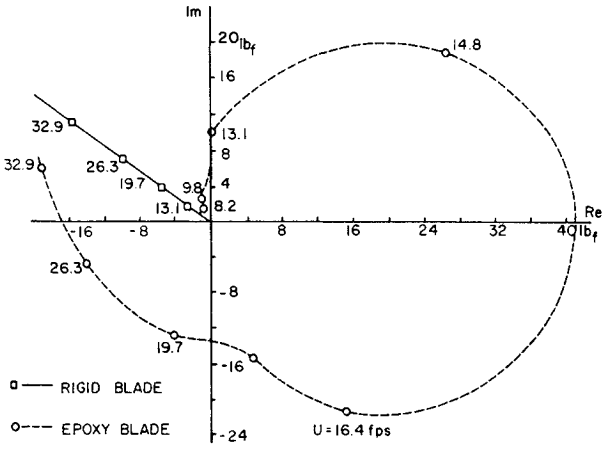

Fig. 6 Amplitudes and phases of the thrust fluctuations of rigid and elastic propellers; $q = 3$ and $q = 6$, $J = 1.15$.

unit—is compared with that of the epoxy resin propeller. The volume mean velocity in the axial direction U is used as a parameter.

In order to check these calculations experimentally the thrust fluctuations exerted by the aluminum and epoxy propellers were measured. The tests were performed in the 48-in.-diam test section of the Water Tunnel located at the Ordnance Research Laboratory of The Pennsylvania State University. Identical flow conditions and instrumentation was used throughout the experiments.

The results are shown in Fig. 7, where the ratio of the magnitude of the unsteady thrust forces exerted by the flexible and rigid propellers are plotted. The theory accurately predicts the velocity at which the peak response occurs. However, a discrepancy between the predicted and measured amplitude ratios exists. In view of the many assumptions in the theory and the uncertainties associated with the measurements, it is difficult to state the precise reasons for this discrepancy. From a practical viewpoint, however, it is immaterial if the thrust fluctuation ratio is equal to 9 as theoretically predicted or 6 as measured, since the propeller must in any event be designed to avoid such a resonance condition in its operating range.

Further calculations were also performed to establish the effects of material properties. Figures 8 and 9 show the results that were obtained.

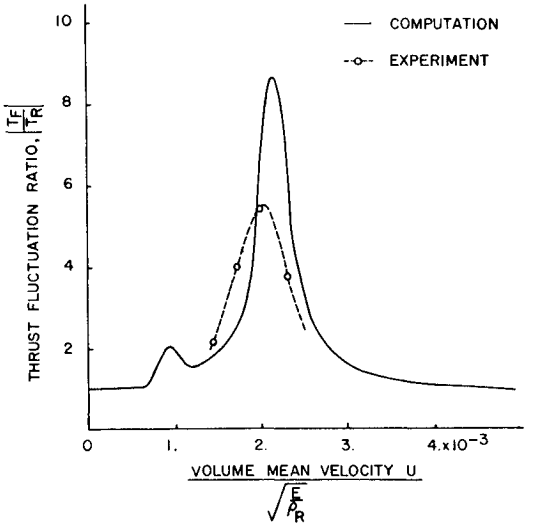

Fig. 7 Thrust fluctuation ratio; $q = 3$ and $q = 6$, $J = 1.15$.

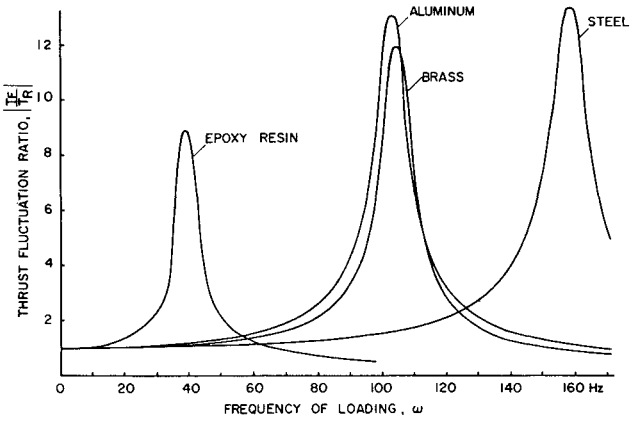

Fig. 8 Thrust fluctuation ratio of the model propeller for various materials; $J = 1.15$; $q = 3$.

Conclusions

Theoretical and experimental investigations such as those of Brown,[1] Tsakonas,[2] Boswell,[3] Yamazaki,[4] Breslin[5] and many others have shown that certain propeller blade geometries lead to a reduction of the magnitudes of the unsteady hydrodynamic forces and moments which cause ship vibrations.

The skewed blade geometries that are suggested by the aforementioned studies, however, possess higher structural flexibilities than the blades of conventional marine propellers. The results obtained in the present study indicate that hydroelastic effects cannot be ignored since substantial magnifications of the forces, torques and moments exerted by the propeller upon a ship's hull may occur.

Appendix A: The Kernel Function

According to Tsakonas[2] $K_1^{\bar{m},\bar{n}}(\gamma_i,\rho_j)$ is given by

1) $\rho_j \neq r_i$ $K_1^{(\bar{m},\bar{n})}(r_i,\rho_j)$

$$= \frac{-1}{\pi r_i^{3/2}} \sum_{m=0}^{\infty}{}', \ {}_N\epsilon_m \sum_{n=1}^{N} f^{(\bar{m},\bar{n})} \int_{\rho_j-\beta}^{\rho_j+\beta} \frac{Q'_{m-1/2}(z)}{\rho^{3/2}} d\rho \quad \text{(A1)}$$

where $Q_{m-\frac{1}{2}}(z)$ denotes Legendre's function of the second kind, of half add-integer order:

$$Q'_{m-1/2}(z) = \frac{\partial}{\partial z} Q_{m-1/2}(z)$$

$$z = \frac{r^2+\rho^2}{2r\rho}, \text{ and } \sum_{n=1}^{N} \bar{f}^{(\bar{m},\bar{n})} \text{ in Appendix B}$$

2) $r_i - 0.01 < \rho < r_i + 0.01$

$$K_1^{(\bar{m},\bar{n})}(r_i,\rho_j) \simeq -\frac{1}{\pi r_i^5} \sum_{m=0}^{\infty}{}', \ {}_N\epsilon_m \sum_{n=1}^{N} \bar{f}^{(\bar{m},\bar{n})} I_2 \quad \text{(A2)}$$

where $\epsilon_m = \begin{cases} 1 \text{ if } m = 0 \\ 2 \text{ if } m = 1, 2, 3 \ldots \end{cases}$

$$I_2 = \frac{2r_i^4}{\beta} - \frac{\beta r_i^2}{8}\left(1.0 + 5.0 \ln 2. - \ln\left(\frac{\beta^2}{2r_i^2}\right)\right), \ \sigma^r = \sigma^\rho \text{ and } \theta_b{}^r = \theta_b{}^\rho$$

for this small region.

$\sum_{n=1}^{N} \bar{f}^{(\bar{m},\bar{n})}$ is given in Appendix B. Note that $\beta = 0.01$ here.

3) $r_i - 0.05 < \rho < r_i - 0.01$ or $r_i + 0.01 < \rho < r_i + 0.05$;

$$K_1^{(\bar{m},\bar{n})}(r_i,\rho_j) = -\frac{1}{\pi r^{3/2}} \sum_{m=0}^{\infty}{}', \ {}_N\epsilon_m \sum_{n=1}^{N} \bar{f}^{(\bar{m},\bar{n})} I_5 \quad \text{(A3)}$$

where

$$I_5 = 2283.2895(f_1 - f_{-1}) + 2397.1028(f_2 - f_{-2}) - 169.02(f_3 - f_{-3}) + 350.9914(f_4 - f_{-4}) + 5.1197(f_5 - f_{-5})$$

$$f_j = \frac{(0.01j)^3}{(r+0.01j)^{3/2}} Q'_{m-1/2}(z_j)$$

$$z_j = \frac{r^2 + (r+0.01j)^2}{2r(r+0.01j)}, \ j = \pm 1, \pm 2, \ldots, \pm 5$$

$K_2^{(\bar{m},\bar{n})}(r_i,\rho_j)$ is given by

$$K_2^{(\bar{m},\bar{n})}(r_i,\rho_j) = 2\beta e^{-\iota q(\sigma^r - \sigma^\rho)} I^{(\bar{m})}(q\theta_b{}^r)\Lambda^{(\bar{n})}(q\theta_r{}^b)F(r,\rho) \quad \text{(A4)}$$

where

$$F(r,\rho) \simeq -\frac{2}{(r\rho)^{1/2}} \frac{a^2}{\theta_0^2}\left[5.94\, Q_{q-1/2}(z_1) - 19.53\, Q_{q-1/2}(z_2) + 13.59\, Q_{q-1/2}(z_3)\right]$$

$$Z_1 = \left[\frac{0.678\bar{\theta}_0}{a} + r^2 + \rho^2\right] /2r\rho$$

$$Z_2 = \left[\frac{1.16\bar{\theta}_0}{a} + r^2 + \rho^2\right] /2r\rho$$

$$Z_3 = \left[\frac{1.30\bar{\theta}_0}{a} + r^2 + \rho^2\right] /2r\rho, \ \bar{\theta}_0 = \frac{2\pi}{N}$$

σ^r and σ^ρ are skewnesses of propeller blade, and where

$$I^{(1)}(X) = J_0(X) - \iota J_1(X)$$

$$I^{(2)}(X) = J_0(X) + \iota J_1(X)$$

$$I^{(\bar{m})}(X) = \frac{\iota^{\bar{m}-1} J_{m-1}(X)}{(\bar{m}-1)}, \ \bar{m} > 2$$

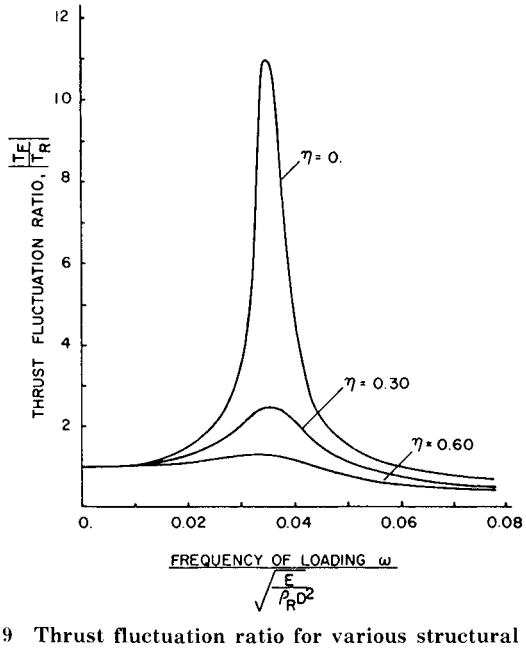

Fig. 9 Thrust fluctuation ratio for various structural damping factors; epoxy propeller, $q = 3$; $J = 1.15$.

$$I_1^{(1)}(X) = -1/2[J_0(X) - J_2(X)] + \iota J_1(X)$$

$$I_1^{(2)}(X) = [J_0(X) - J_2(X)] + \iota J_1(X)$$

$$I_1^{(\bar{m})}(X) = \frac{\iota(\bar{m}-2)}{2(\bar{m}-1)}[-J_{\bar{m}}(X) + J_{\bar{m}-2}(X)],\ \bar{m} > 2 \quad \text{(A5)}$$

$$\Lambda^{(1)}(X) = J_0(X) - \iota J_1(X)$$

$$\Lambda^{(\bar{n})}(X) = \frac{(-\iota)^{\bar{n}-2}}{2(\bar{n}-1)}[J_{\bar{n}-2}(X) + J_{\bar{n}}(X)],\ \bar{n} > 1$$

$$\Lambda_1^{(1)}(X) = \frac{1}{2}[J_0(X) - J_2(X)] - \iota J_1(X)$$

$$\Lambda_1^{(\bar{n})}(X) = \frac{(-\iota)^{\bar{n}+1}}{4(\bar{n}-1)}[J_{\bar{n}-3}(X) - J_{\bar{n}+1}(X)],\ \bar{n} > 1 \quad \text{(A6)}$$

$J_n(X)$ = Bessel Function of the first kind, or order n.

Appendix B: Evaluation of $\sum_{n=1}^{N} \bar{f}^{(\bar{m},\bar{n})}$

$$\sum_{n=1}^{N} \bar{f}^{(\bar{m},\bar{n})} = N \left\{\left[\frac{\bar{\theta}_0}{2} + (\sigma^r - \sigma^p)\right] I^{(\bar{m})}(0)\Lambda^{(\bar{n})}(0) - \theta_b{}^r I_1^{(\bar{m})}(0)\Lambda^{(\bar{n})}(0) + \theta_b{}^p I^{(\bar{m})}(0)\Lambda_1^{(\bar{n})}(0)\right\} \text{ for } m = q = 0, \quad \text{(B1)}$$

$$= \frac{N}{2}\left\{e^{-\iota q(\sigma^r-\sigma^p)} I^{(\bar{m})}(q\theta_b{}^r)\Lambda^{(\bar{n})}(q\theta_b{}^p)\left[\frac{\bar{\theta}_0}{2} + \sigma^r - \sigma^p + \frac{\iota e^{-\iota q\bar{\theta}_0}}{2q}\right] - \frac{\iota e^{-\iota q(\sigma^r-\sigma^p)}}{2q} I^{(\bar{m})}(-q\theta_b{}^r)\Lambda^{(\bar{n})}(-q\theta_b{}^p) + e^{-\iota q(\sigma^r-\sigma^p)} - \theta_b{}^r I_1^{(\bar{m})}(q\theta_b{}^r)\Lambda^{(\bar{n})}(q\theta_b{}^r) + \theta_b{}^p I^{(\bar{m})}(q\theta_b{}^r)\Lambda_1^{(\bar{n})}(q\theta_b{}^p)\right\} \quad \text{(B2)}$$

for $m = q \neq 0$

$$= \frac{\iota N}{2}\left\{e^{-\iota q(\sigma^r-\sigma^p)} I^{(\bar{m})}(q\theta_b{}^r)\Lambda^{(\bar{n})}(q\theta_b{}^p)\left[\frac{e^{-\iota(m+q)\bar{\theta}_0/2}}{m+q} - \frac{e^{\iota(m-q)\bar{\theta}_0/2}}{m-q}\right] + e^{-\iota m(\sigma^r-\sigma^p)} I^{(\bar{m})}(m\theta_b{}^r)\Lambda^{(\bar{n})}(m\theta_b{}^p) - \frac{e^{\iota m(\sigma^r-\sigma^p)}}{m+q} I^{(\bar{m})}(-m\theta_b{}^r)\Lambda^{(\bar{n})}(-m\theta_b{}^p)\right\} \quad \text{(B3)}$$

for $m \neq q$

These equations are reproduced from Ref. 2.

References

[1]Brown, N. A., "Periodic Propeller Forces in Nonuniform Flow," Rept 64-7, 1964, MIT, Cambridge, Mass.

[2]Tsakonas, S., Jacobs, W. R., and Rank, P. H., Jr., "Unsteady Propeller Lifting-Surface Theory," R-1133, 1966, Stevens Institute of Technology, Hoboken, N. J.

[3]Watkins, C. E., Woolston, D. S., and Cunningham, H. J., "A Systematic Kernel Function Procedure for Determining Aerodynamic Forces on Oscillating or Steady Finite Wings at Subsonic Speeds," TR R-48, 1959, NASA.

[4]Tsushima, H., "Dynamic Response of an Elastic Propeller to a Nonuniform Inflow," Ph.d. thesis, 1972, Dept. of Aerospace Engineering, The Pennsylvania State University, University Park, Pa.

[5]Boswell, R. J., "Measurements, Correlation with Theory, and Parametric Investigation of Unsteady Propeller Forces and Moments," M.S. thesis, Aug. 1967, Dept. of Aerospace Engineering, The Pennsylvania State University, University Park, Pa.

[6]Yamazaki, R., "On the Theory of Screw Propellers in Nonuniform Flows," *Memoirs of the Faculty of Engineering, Kyushu University*, Vol. 25, No. 2, 1966, pp. 1082–1096.

[7]Breslin, J. P., "Exciting-Force Operators for Ship Propellers," *Journal of Hydronautics*, Vol. 5, No. 3, July 1971, pp. 85–90.